

Galaxy UV-luminosity function and reionization constraints on axion dark matter

Brandon Bozek^{1,2*}, David J. E. Marsh³, Joseph Silk^{2,4,5}, Rosemary F.G. Wyse².

¹*Department of Astronomy and Joint Space-Science Institute, University of Maryland, College Park, MD 20742, USA*

²*Department of Physics and Astronomy, The Johns Hopkins University, Homewood Campus, Baltimore MD 21218, USA*

³*Perimeter Institute, 31 Caroline St N, Waterloo, ON, N2L 6B9, Canada*

⁴*Institut d'Astrophysique, UMR 7095 CNRS, Université Pierre et Marie Curie, 98bis Blvd Arago, 75014 Paris, France*

⁵*Beecroft Institute of Particle Astrophysics and Cosmology, Department of Physics, University of Oxford, Oxford OX1 3RH, UK*

1 March 2018

ABSTRACT

If the dark matter (DM) were composed of axions, then structure formation in the Universe would be suppressed below the axion Jeans scale. Using an analytic model for the halo mass function of a mixed DM model with axions and cold dark matter, combined with the abundance-matching technique, we construct the UV-luminosity function. Axions suppress high- z galaxy formation and the UV-luminosity function is truncated at a faintest limiting magnitude. From the UV-luminosity function, we predict the reionization history of the universe and find that axion DM causes reionization to occur at lower redshift. We search for evidence of axions using the *Hubble Ultra Deep Field* UV-luminosity function in the redshift range $z = 6\text{--}10$, and the optical depth to reionization, τ , as measured from cosmic microwave background polarization. All probes we consider consistently exclude $m_a \lesssim 10^{-23}$ eV from contributing more than half of the DM, with our strongest constraint ruling this model out at more than 8σ significance. In conservative models of reionization a dominant component of DM with $m_a = 10^{-22}$ eV is in 3σ tension with the measured value of τ , putting pressure on an axion solution to the cusp-core problem. Tension is reduced to 2σ for the axion contributing only half of the DM. A future measurement of the UV-luminosity function in the range $z = 10\text{--}13$ by *JWST* would provide further evidence for or against $m_a = 10^{-22}$ eV. Probing still higher masses of $m_a = 10^{-21}$ eV will be possible using future measurements of the kinetic Sunyaev–Zel’dovich effect by Advanced ACTPol to constrain the time and duration of reionization.

Key words: elementary particles – galaxies: high-redshift – galaxies: luminosity function, mass function – cosmology: theory – dark ages, reionization, first stars – dark matter.

1 INTRODUCTION

While dark matter (DM) is known to comprise a large portion of the energy density of the universe, $\Omega_d h^2 \approx 0.12$ (e.g. Planck Collaboration XVI 2014b), and plays an important role in the formation and dynamics of galaxies and clusters, its particle nature is unknown. Two leading candidates in well-motivated and minimal

extensions of the standard model of particle physics (the SM) are weakly-interacting massive particles (WIMPs), which emerge naturally in supersymmetry (Jungman, Kamionkowski & Griest 1996), and the QCD axion (Peccei & Quinn 1977; Weinberg 1978; Wilczek 1978), which solves the CP problem of strong interactions. Many experimental efforts are underway to detect and constrain these DM candidates via their direct (e.g. Asztalos et al. 2010; Aalseth et al. 2011; Aprile et al. 2012; Agnese et al. 2014; Akerib et al. 2014; Angloher et al.

* bbozek@astro.umd.edu

2014; Budker et al. 2014; Stadnik & Flambaum 2014) or indirect (e.g. Brockway, Carlson & Raffelt 1996; Grifols, Masso & Toldra 1996; Ackermann et al. 2011; Abbasi et al. 2012; Aguilar et al. 2013; Friedland, Giannotti & Wise 2013; Blum et al. 2014) interactions with the SM, but no definitive evidence has so far emerged.¹

As these experiments designed to directly detect WIMPs and axions continue to report null results (Beringer et al. 2012; Akerib et al. 2014), with associated shrinkage of allowed parameter space, we are motivated to try to constrain the particle nature of DM via the only interaction it is known to have: gravitation. Further, we will explore models beyond those where WIMPs and axions comprise all of the DM and consider scenarios where the DM is multi-component.

We can go further than measuring the DM density and can constrain the physics of DM should it affect the formation and growth of structure in a novel way. Cold (C)DM clusters on all scales and makes well-understood predictions relating to the formation and growth of cosmic structure (Peebles 1971; Bond & Szalay 1983; Blumenthal et al. 1984; Davis et al. 1985). Standard supersymmetric WIMPs have $\mathcal{O}(\text{GeV})$ masses and are thermally produced, leading to negligible free-streaming lengths – the defining characteristic of cold dark matter (CDM). The QCD axion is much lighter than a WIMP, with $\mathcal{O}(\mu\text{eV})$ mass but, since it is non-thermally produced, it too is gravitationally indistinguishable from CDM due to vanishing sound-speed (e.g. Noh, Park & Hwang 2013). Since both standard WIMPs and QCD axions are equivalent to CDM in structure formation,² in order to learn about the particle nature of DM via gravitational probes it must cluster in a manner distinct from CDM. Constraining the particle nature of DM using the growth of structure therefore requires considering models other than standard WIMPs and the QCD axion.

2 PROBING THE NATURE OF DM USING STRUCTURE FORMATION

2.1 Models, motivations, and existing bounds

Two popular models that manifest novel structure formation are warm (W)DM (e.g. Bond, Szalay & Turner 1982; Bode, Ostriker & Turok 2001) and ultralight axions (ULAs, e.g. Arvanitaki et al. 2010). The low-mass

scale necessary for ULAs can be naturally realized in string theory models (e.g. Acharya, Bobkov & Kumar 2010; Cicoli, Goodsell & Ringwald 2012), or in the hidden-sector model of Chiueh (2014). Alternatively it could occur for the QCD axion with an extremely super-Planckian decay constant, but this is considered theoretically problematic (e.g. Arkani-Hamed et al. 2007).

Each of these models has additional motivation since both WDM and ULAs suppress small-scale structure and can help in the resolution of the small-scale problems of CDM, which include the over-prediction of low-mass dark haloes (‘missing satellites’; Moore et al. 1999; Klypin et al. 1999); the prediction of a central ‘cusp’ in the DM density profile while observations favour ‘cores’ (Wyse & Gilmore 2008); the prediction of more numerous satellite galaxies of the mass of the Large Magellanic Clouds (the ‘too-big-too-fail’ problem; Boylan-Kolchin, Bullock & Kaplinghat 2011) and the difficulty in producing typical disc galaxies due to the prediction of active mergers until redshift of order unity (Wyse 2001).

The adoption of a lower mass thermally produced DM particle, such as in the WDM scenario, introduces a tension between the desire to produce a core in the inner regions of the DM density profile – favouring a lower mass, while simultaneously producing dwarf galaxies in sufficient number – favouring a higher mass (Macciò et al. 2013; Schneider et al. 2014). Other effects of WDM, in the case of an $\sim 1\text{keV}$ neutrino, include a significant impact on faint galaxy counts (Schultz et al. 2014) and early star formation rates (Dayal, Mesinger & Pacucci 2014).

Following the work of Hu, Barkana & Gruzinov (2000), it was shown in Marsh & Silk (2013) that ULAs are not subject to this tension due to the inverse relationship between halo mass and core size in these models. Recently, high-resolution simulations of core formation with ULAs by Schive, Chiueh & Broadhurst (2014); Schive et al. (2014b) have confirmed this picture. Fits to the cored halo profile in Fornax give a best-fitting mass of $m_a = 8.1^{+1.6}_{-1.7} \times 10^{-23}$ eV, providing a large core while still forming low-mass galaxies.

Cosmological probes of the linear regime of structure formation, such as the power spectrum, $P(k)$, of density fluctuations (e.g. Reid et al. 2010) and the cosmic microwave background (CMB; e.g. Planck Collaboration I 2014a), provide only weak constraints on the mass of the DM particle (warm or axion-like) in each of these scenarios.³ The WDM cannot be ‘too warm’, for example we must have $m_W \gtrsim 0.1$ keV, and ULAs can-

¹ The particle physics status of DM, including LHC searches for supersymmetric WIMPs, is reviewed in Beringer et al. (2012). For reviews of axion physics see Raffelt (2002) and Wantz & Shellard (2010). Of course supersymmetry and axions are not mutually exclusive: indeed they are necessary partners in string theory (Witten 1984; Svrcek & Witten 2006). For a review of DM models with supersymmetric axions see Baer et al. (2014).

² If axion DM were to form a Bose-Einstein condensate, then some features such as vortices or caustics in galaxies may occur (e.g. Sikivie 2011).

³ From structure formation it is well established that that the DM is not ‘hot’, for example composed of light neutrinos (Tremaine & Gunn 1979; Bond, Szalay & Turner 1982; White, Frenk & Davis 1983). For DM composed of CDM plus massive neutrinos, the CMB limits the total neutrino mass as $\sum m_\nu < 0.66$ eV at 95 per cent C.L. (Planck Collaboration XVI 2014b) and neutrinos contribute a sub-per cent fraction of DM.

not be too light either, $m_a \gtrsim 10^{-24}$ eV (Amendola & Barbieri 2006, Marsh et al., in preparation). However, since one requires $m_W \sim \mathcal{O}(1)$ keV and $m_a \sim 10^{-22}$ eV in order for WDM or ULAs to be relevant to the small-scale problems, linear probes are silent on the validity of these scenarios.

Thus, in order to test and constrain a particle physics solution to the small-scale problems, we must look to non-linear probes of structure formation. One such probe is the Ly α forest flux power spectrum. Viel et al. (2013) have used observations of the Ly α forest, combined with hydrodynamic simulations of structure formation, to place the strongest constraint to date on WDM, $m_W > 3.3$ keV. Amendola & Barbieri (2006) used older Ly α data to constrain ULAs, placing the bound $m_a > 5 \times 10^{-23}$ eV if the ULA is to be all of the DM. Analyses of the Ly α forest involve considerable complexity related to the non-linear mapping of the optical depth and to the required calibration from simulations involving gas physics. No detailed predictions have been made for the Ly α forest with ULAs as DM, as such simulations do not exist. Existing Ly α constraints on WDM and ULAs point to larger masses of the scale we hope to constrain, and if properly understood will be able to provide consistency and cross-checks.⁴

2.2 The UV-luminosity function and reionization

The two probes we will focus on in this work are one, the UV-luminosity function of galaxies at high-redshift, $\phi(z)$, as measured by the *Hubble Space Telescope* e.g. Bouwens et al. (2014) and two, the reionization history of the universe through the Thomson scattering optical depth to reionization, τ , measured from large-angle CMB polarization by *WMAP* (Bennett et al. 2013).⁵

The extremely deep imaging in bandpasses from the optical to near-IR with the *Hubble Space Telescope* (*HST*) available in several Legacy Fields provides the most fundamental data set for constraining the contribution of galaxies to the reionization of the universe through estimation of the rest-frame UV-luminosity function over the redshift range between $z = 4$ and 10 (Bouwens et al. 2011, 2014; Oesch et al. 2012; Lorenzoni et al. 2013; McLure et al. 2013). The rest-frame UV-luminosity function is a measure of the number density, per absolute magnitude, of the star-forming galax-

ies that are likely to be the primary driver of reionization (Madau, Haardt & Rees 1999; Bunker et al. 2004; Yan & Windhorst 2004; Oesch et al. 2009; Kuhlen & Faucher-Giguère 2012; Robertson et al. 2013). Other possible sources of reionization, such as quasars and annihilating DM, have little observational support and would in any case still require, at a minimum, a sizeable contribution from star-forming galaxies to maintain reionization (Haiman & Loeb 1998; Belikov & Hooper 2009; Willott et al. 2010; Fontanot, Cristiani & Vanzella 2012).

There are a variety of constraints on the epoch of reionization (for a summary of current constraints see Robertson et al. 2013); here we will focus on the observations of the Gunn-Peterson trough (Gunn & Peterson 1965) in quasar spectra (Fan et al. 2006) and the analysis of the covering fraction of ‘dark’ pixels in quasar spectra (Mesinger 2010; McGreer, Mesinger & Fan 2011) that constrains the neutral fraction at the end of reionization, plus the Thompson scattering optical depth of CMB photons that provides an integral constraint over the full history of reionization. These constraints taken together with the UV-luminosity function argue for an extended period of reionization that begins early in cosmic time.

Star-forming galaxies during the epoch of reionization must have a significant ionizing-photon escape fraction and the UV galaxy luminosity function must extend beyond the observed limits in both intrinsic luminosity and redshift in order for galaxies to reionize the universe (Kuhlen & Faucher-Giguère 2012; Robertson et al. 2013). The assumed forms of, and values for, the parameters used to model reionization – the redshift evolution of the UV-luminosity function, the limiting luminosity at which galaxy formation is assumed to truncate, and the escape fraction of ionizing photons – have a large impact on the derived reionization history. Within the CDM paradigm, there exists an interesting tension between the suppression of star formation in low-mass DM haloes which is necessary to match near-field observations, such as the luminosity function and spatial distribution of the Milky Way satellite galaxies, with the expectation of low-mass galaxies at high redshift to be the dominant source of reionization (Boylan-Kolchin, Bullock & Garrison-Kimmel 2014).

As already discussed WDM is a possible solution to CDM small-scale issues in the local Universe. Recently, Schultz et al. (2014) used the predicted high redshift UV-luminosity functions, reionization history, and CMB optical depth to constrain the mass of a thermally produced WDM particle, ruling out $m_W = 1.3$ keV at greater than 2σ and suggesting sensitivity of future experiments to $m_W = 2.6$ keV. In this paper, we follow the approach of Schultz et al. (2014) in using an abundance-matching technique, albeit with a modified procedure that we describe, to predict the high-redshift UV-luminosity functions, reionization history, and CMB optical depth of axion Mixed Dark Matter (aMDM) models and compare those predictions to reionization constraints from observations.

⁴ Another probe that can constrain non-linear scales is galaxy weak lensing, for example through the anticipated data sets from *Euclid* (Laureijs et al. 2011; Amendola et al. 2013). Smith & Markovic (2011) forecast that *Euclid* may be able to constrain $m_W \gtrsim 2.6$ keV, and prospects for ULAs also look promising (Marsh et al. 2012, Marsh, in preparation), though considerable experimental and theoretical systematics are involved.

⁵ We use the τ likelihood derived from *Planck*+*WMAP* chains in Spergel, Flauger & Hlozek (2013).

3 ULTRALIGHT AXION DM

We begin this section with a simple argument that relates the relevant mass scales for ULAs and WDM, and then give more details of our semi-analytic model for the ULA mass function.

3.1 Thermal and non-thermal scales

Structure formation at late times and on the largest scales constrains the dominant component of the DM to have growth $\delta \sim a$, where a is the Friedmann–Robertson–Walker scale factor, so that the power spectrum and growth on these largest scales is the same as for CDM. If the DM is not completely cold and pressureless for all of cosmic history, with equation of state $w = P/\rho = 0$ and sound speed $c_s^2 = \delta P/\delta\rho = 0$, then scales can be imprinted on structure formation corresponding to the horizon size when any particular change occurred in these quantities. This scale can be used to suppress the formation of small-scale structure relative to CDM, and thus in hierarchical structure formation suppress the formation of high-redshift galaxies and the onset of reionization.

With WDM (for example a thermal gravitino as in Bond, Szalay & Turner 1982) the relevant scales are fixed by the temperature, T . The equation of state transitions from $w = 1/3$ to $w = 0$ when the WDM becomes non-relativistic, and structure is suppressed on scales of order the horizon size when $T \sim m_W$. If the DM is non-thermal, as for a ULA or other ultralight scalar, then the relevant scale is the Hubble scale, H . The (time averaged) equation of state transitions from $w_a = -1$ to 0 when the axion mass overcomes Hubble friction in the Klein–Gordon equation, and structure is suppressed on scales of order the horizon when $H \sim m_a$ (e.g. Hu, Barkana & Gruzinov 2000; Amendola & Barbieri 2006; Marsh & Ferreira 2010).

Scales corresponding to dwarf galaxies were horizon size during the radiation dominated era. During this time the temperature is related to the Hubble scale by

$$T \sim \sqrt{HM_{\text{pl}}}, \quad (1)$$

where $M_{\text{pl}} = 1/\sqrt{8\pi G} = 2.4 \times 10^{18}$ GeV is the reduced Planck mass. As already discussed, WDM with (thermal equivalent) mass $m_W \sim \mathcal{O}(1)$ keV is a viable candidate to constitute a large fraction of the DM, and may play a role in resolution of the small-scale problems of CDM. If an axion is to affect structure on similar scales, then a simple order of magnitude estimate for the required axion mass is found by relating $T \sim m_W$ and $T \sim (HM_{\text{pl}})^{1/2} \sim (m_a M_{\text{pl}})^{1/2}$: one finds $m_a \sim 10^{-21}$ eV.

Axions and other light scalar fields with mass in the range 10^{-24} eV $\lesssim m_a \lesssim 10^{-20}$ eV have been called ‘Fuzzy’ (F)CDM (Hu, Barkana & Gruzinov 2000). A more detailed study using the full linear transfer function shows that this range of ULA mass affects structure

formation on the same scales as WDM with mass in the range $0.1 \text{ keV} \lesssim m_W \lesssim 4 \text{ keV}$ (Marsh & Silk 2013).

3.2 The growth of structure and the halo mass function

Here, we present the Sheth–Tormen (Sheth & Tormen 1999) mass function for aMDM including scale-dependent growth: for more details see Marsh & Silk (2013). The transfer functions and growth factor we use are computed using a modified version of CAMB (Lewis & Challinor 2000) which includes light axions and will be described in Marsh et al. (in preparation).

The axion field, ϕ , evolves according to the Klein–Gordon equation with a quadratic potential,⁶ $V(\phi) = m_a^2 \phi^2/2$. When the field is oscillating about the potential minimum at times $t > t_{\text{osc}}$, where $H(t_{\text{osc}}) \sim m_a$ one can show that the equation of state and sound speed in the effective fluid description (Hu 1998) averaged on time periods $t > 1/m_a$ are given by (e.g. Turner 1983; Hu, Barkana & Gruzinov 2000; Park, Hwang & Noh 2012)

$$w_a = 0, \quad (2)$$

$$c_s^2 = \frac{k^2/4m_a^2 a^2}{1 + k^2/4m_a^2 a^2}. \quad (3)$$

With these prescriptions for the equation of state and sound speed, in a universe dominated by axions at late times, the axion overdensity, $\delta_a = \delta\rho_a/\bar{\rho}_a$, evolves (in the Newtonian gauge and in conformal time) according to (Ma & Bertschinger 1995)

$$\ddot{\delta}_a + \mathcal{H}\dot{\delta}_a + (k^2 c_s^2 - 4\pi G a^2 \bar{\rho}_a)\delta_a = 0, \quad (4)$$

where $\mathcal{H} = aH$ is the conformal Hubble rate and over-dots denote derivatives with respect to conformal time, η . For small k , the sound speed goes to zero and we recover scale-independent linear growth, with $\delta_a \sim a$ on large scales. However, for large k the sound speed dominates and the overdensity oscillates rather than grows. The transition between growth and oscillation occurs at the Jeans scale

$$k_J = a(16\pi G \bar{\rho}_a)^{1/4} m_a^{1/2}. \quad (5)$$

For $k > k_J$ there is no growth of structure. There is scale-dependent growth as k decreases from k_J , continuously interpolating to the standard scale-independent linear growth on the largest scales, $k \ll k_J$ (Khlopov, Malomed & Zeldovich 1985).

In the halo mass function (HMF) one can use the variance of the matter power spectrum, $\sigma(M)$, computed at redshift $z = 0$ if the barrier for collapse, δ_c , is given by the Einstein-de Sitter value at $z = 0$,

⁶ This is true near the minimum for the full potential, which is periodic in ϕ . We ignore anharmonic effects which can be shown to have negligible effect on the Jeans scale for the range of masses we consider (Boyle, Caldwell & Kamionkowski 2002).

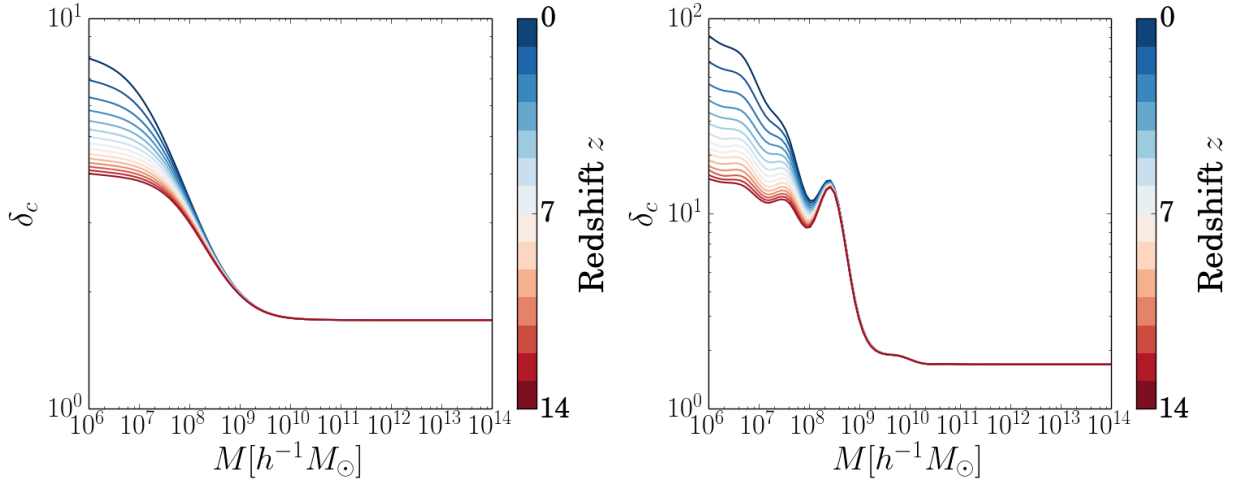


Figure 1. The mass-dependent critical overdensity for two benchmark models in which some or all of the DM is in the form of ULAs, shown for each redshift in the range $0 \leq z \leq 14$. Left-hand panel: $m_a = 10^{-22}$ eV, $\Omega_a/\Omega_d = 0.5$. Right-hand panel: $m_a = 10^{-22}$ eV, $\Omega_a/\Omega_d = 1$.

$\delta_{c,\text{EdS}} \approx 1.686$, scaled by the linear growth: $\delta_c(z) = \delta_{c,\text{EdS}}/D(z)$. Marsh & Silk (2013) proposed that one could account for scale-dependent growth by simply replacing $D(z) \rightarrow D(k, z)$ and then using the enclosed mean mass to define a halo-mass-dependent barrier for collapse, $\delta_c(M, z)$.

Fig. 1 shows $\delta_c(M, z)$ computed in this manner for two aMDM cosmologies, which can be considered as benchmarks for the purposes of this paper. They each take $m_a = 10^{-22}$ eV while varying the fractional energy density in axions, $\Omega_a = \rho_a/\rho_{\text{crit}}$, and CDM, Ω_c , and holding the total DM density, $\Omega_d = \Omega_a + \Omega_c$, fixed. The first model takes $\Omega_a/\Omega_d = 0.5$, so that half of the DM is in ULAs, and the second takes $\Omega_a/\Omega_d = 1$. As may be seen in the figure, the barrier for collapse becomes large for low-mass objects due to the vanishing growth on scales below the Jeans scale. This is consistent with what is found from an excursion-set calculation by Benson et al. (2013) applied to WDM at the WDM Jeans scale.

The mass-dependent barrier for collapse can simply be substituted into the Sheth–Tormen mass function along with the correct variance to find $dn/d \ln M$, the number density of haloes per logarithmic mass bin. The HMFs for the two benchmark cosmologies of Fig. 1 are shown in Fig. 2. The rising value of $\delta_c(M)$ for low M is seen to suppress the HMF relative to CDM in both cosmologies, particularly at high- z . The existence of this sharp suppression due to scale-dependent growth is both a key prediction of aMDM and the primary means with which we will constrain it. At high redshift, we should expect many fewer objects to have formed when the DM contains a ULA compared to a pure CDM universe, even when ULAs are only a fractional component of the DM.

The cut-off in the HMF at $z = 13$ in Fig. 2 (right-hand panel) occurs at $M \approx 10^9 h^{-1} M_\odot$, and the HMF

peaks near this value. This is consistent with the high-resolution simulations of the formation of structure in a universe dominated by axion DM with $m_a = 8.1 \times 10^{-23}$ eV carried out by Schive, Chiueh & Broadhurst (2014) that report a first object of mass $M = 10^9 M_\odot$ at $z = 13$. While Schive, Chiueh & Broadhurst (2014) do not report the full HMF from their simulations, we find this quantitative agreement encouraging as a validation of our semi-analytic model.

4 UV-LUMINOSITY FUNCTIONS AND THE ABUNDANCE MATCHING TECHNIQUE

We use the abundance-matching technique (Kravtsov et al. 2004; Vale & Ostriker 2004) to connect the aMDM HMFs discussed in Section 3 to high-redshift rest-frame UV-luminosity functions determined from deep imaging in optical to near-IR bandpasses of *HST* Legacy Fields (Bouwens et al. 2014 and references therein). The abundance-matching technique assigns a galaxy of a given absolute rest-frame UV (1500 Å) magnitude, M_{UV} (we will use AB-magnitudes for the purposes of comparisons with observational data), to a given DM halo mass, M_h , by assuming that each DM halo hosts one galaxy and that the relationship between dark-matter halo mass and galaxy luminosity, $M_h(M_{\text{UV}})$, is monotonic.

The first step in this matching process is characterization of the galaxy luminosity function (the number density of galaxies per absolute magnitude), $\phi(M)$, by fitting a suitable analytic function to the *HST* galaxy number counts at redshifts $z = 6$ –10. We adopt the usual practice of fitting a Schechter function (Schechter

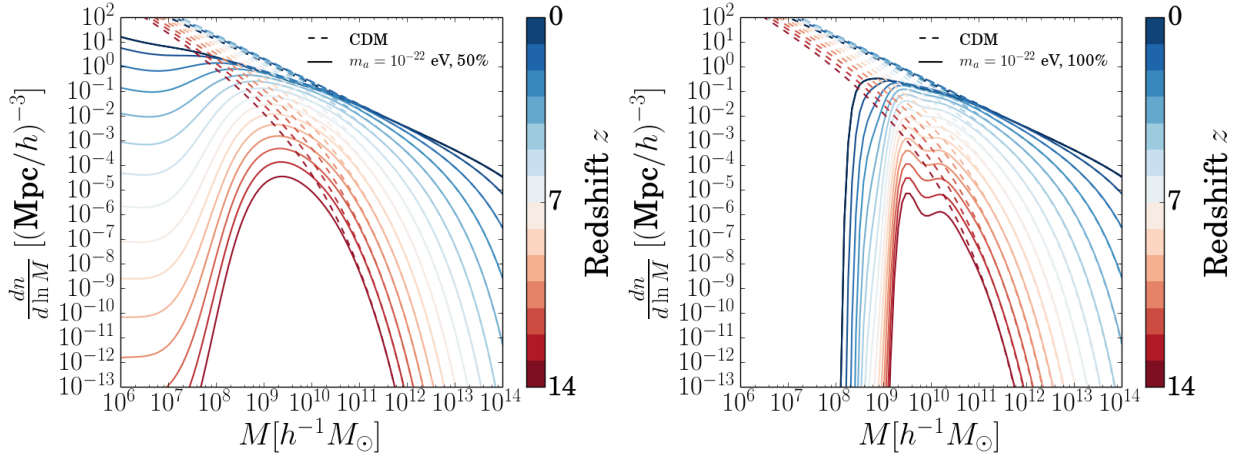


Figure 2. Sheth-Tormen mass function for ULAs including scale-dependent growth, shown for each redshift in the range $0 \leq z \leq 14$. The result for CDM is shown for reference. Left-hand panel: $m_a = 10^{-22}$ eV, $\Omega_a/\Omega_d = 0.5$. Right-hand panel: $m_a = 10^{-22}$ eV, $\Omega_a/\Omega_d = 1$.

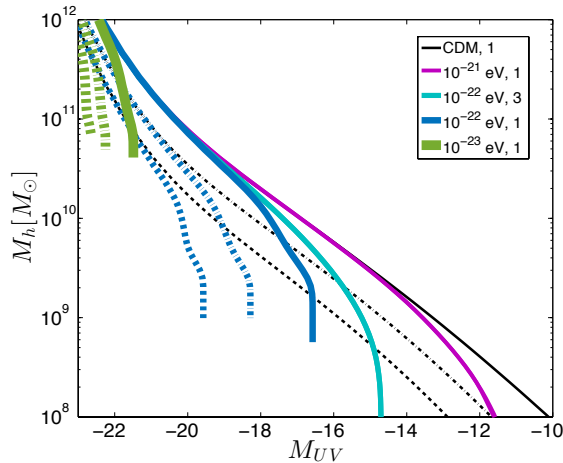


Figure 3. The DM halo mass–galaxy luminosity relation, $M_h(M_{UV})$, for CDM (black) and aMDM models $\{m_a = 10^{-21}$ eV, ‘1’ (purple); $m_a = 10^{-22}$ eV, ‘3’ (cyan); $m_a = 10^{-22}$ eV, ‘1’ (blue); $m_a = 10^{-23}$ eV, ‘1’ (green) $\}$ at redshifts $z = 7$ (solid curve), $z = 10$ (dot–dashed), and $z = 13$ (dashed). The truncation in the $M_h(M_{UV})$ relation for models $m_a = 10^{-22}$ eV, ‘1’ and $m_a = 10^{-23}$ eV, ‘1’ is due to a truncation in the corresponding HMF (as shown in the right-hand panel of Fig. 2). The turnover in the $M_h(M_{UV})$ relation in the $m_a = 10^{-22}$ eV, ‘3’ model at $z = 7$ is the result of a turnover (without a complete truncation) in the $m_a = 10^{-22}$ eV, $\Omega_a/\Omega_d = 0.5$ HMF at $z = 7$ (left-hand panel of Fig. 2).

1976) which has the following form:

$$\phi(M) = \phi_\star \left(\frac{\ln(10)}{2.5}\right) 10^{-0.4(M-M_\star)\alpha} \exp(-10^{-0.4(M-M_\star)}), \quad (6)$$

where ϕ_\star is the normalization, M_\star is the characteris-

tic magnitude, α is the faint-end slope, and M_{UV} is used when applying equation (6). We use two sets of Schechter function parameters, respectively, taken from Bouwens et al. (2014) and Kuhlen & Faucher-Giguère (2012) (their ‘FIT’ model), since different values for the Schechter function parameters (particularly the faint-end slope) can have a significant effect on the resulting reionization history. Each Schechter function fit is extrapolated to fainter magnitudes and redshifts where there are not currently observations by assuming the values of the parameters evolve linearly with redshift consistent with the trends in the data at redshifts 6–10 (see the above cited works for the model details). The data that the Bouwens et al. (2014) luminosity function is based on includes more recent data than that of Kuhlen & Faucher-Giguère (2012), but both models are consistent with the current data set.

The parametrized fit to the observed galaxy luminosity function and the DM HMF of a given model are, at each redshift, integrated to obtain, respectively, the cumulative galaxy luminosity function, $\Phi(< M_{UV})$, the number density of galaxies brighter than M_{UV} and the cumulative DM HMF, $n(> M_h)$, the number density of haloes more massive than M_h . For each DM model, an absolute magnitude, M_{UV} , is assigned to a dark matter halo mass, M_h by matching number densities in the cumulative functions, i.e. according to the relation:

$$\Phi(< M_{UV}, z) = n(> M_h, z). \quad (7)$$

This gives the DM halo mass–galaxy luminosity relations, $M_h(M_{UV})$, shown in Figure 3. The $M_h(M_{UV})$ relation is then used to convert the cumulative DM mass function of a given model into a predicted cumulative galaxy luminosity function.

This may appear to be a circular process but the predicted cumulative luminosity function for each DM model will match exactly with the input cumulative

galaxy luminosity function derived from observations only provided that the DM HMF actually contain low-mass haloes of a sufficient (cumulative) number density to match the faint end of the observed luminosity function – otherwise the predicted luminosity function will end prematurely compared to observations.

Indeed, a truncation in the HMF at some minimum halo mass, as shown in the right-hand panel of Fig. 2, leads to a corresponding truncation in the $M_h(M_{UV})$ relation, as is clearly seen for the $m_a = 10^{-22}$ eV, Model 1 (100 per cent axion DM), case in Fig. 3. For the case of a turnover in the HMF without a complete truncation, as shown in the left-hand panel of Fig. 2, the $M_h(M_{UV})$ relation will steepen such that several orders of magnitude in DM halo mass maps on to a nearly singular value of galaxy luminosity, as can be seen for the $m_a = 10^{-22}$ eV, Model 3 (50 per cent axion DM), case in Fig. 3. A truncation will occur in the resulting aMDM cumulative luminosity function at the corresponding magnitude for both cases. The terminal value in the aMDM cumulative luminosity function, therefore, indicates the minimum mass scale of galaxy formation at each redshift based on whether a sufficient number of DM haloes of that mass scale have collapsed.

The advantage of the abundance-matching procedure is that it provides a pathway to constraining DM mass functions by directly comparing to galaxy observations without appealing to uncertain galaxy formation physics. The $M_h(M_{UV})$ relation additionally serves as a prediction for validation or rejection of a given theory.

Schultz et al. (2014) used a different methodology in their abundance-matching procedure for the WDM case. Those authors used the $M_h(M_{UV})$ relation obtained from the CDM abundance-matching when constructing the predicted WDM cumulative luminosity functions. Their argument for this choice was the unknown galaxy formation physics that accounts for their $M_h(M_{UV})$ relation should be based on CDM, as WDM mass functions would require a more efficient galaxy formation process in low-mass galaxies. Our approach uses the same DM mass function at the beginning and end of the abundance-matching procedure, which we consider to be more self-consistent.

5 REIONIZATION

We determine the reionization history of aMDM models, as represented by the volume-filling fraction of ionized hydrogen, $Q_{\text{HII}}(z)$. The volume-filling fraction of ionized hydrogen balances the ionization of the neutral intergalactic medium (IGM) with the recombination of free electrons and protons, as given by the differential equation (Madau, Haardt & Rees 1999; Kuhlen & Faucher-Giguère 2012; Robertson et al. 2013; Schultz et al. 2014):

$$\frac{dQ_{\text{HII}}}{dt} = \frac{\dot{n}_{\text{ion}}}{\bar{n}_{\text{H}}} - \frac{Q_{\text{HII}}}{\bar{t}_{\text{rec}}}, \quad (8)$$

where the \bar{n}_{H} term represents the mean comoving hydrogen number density and \dot{n}_{ion} is the comoving production

rate of ionizing photons per unit volume. The parameter \bar{t}_{rec} is the volume-averaged recombination time of ionized hydrogen given by the equation:

$$\bar{t}_{\text{rec}} = \frac{1}{C_{\text{HII}}\alpha_B(T_0)\bar{n}_{\text{H}}(1+Y/4X)(1+z)^3}, \quad (9)$$

where $C_{\text{HII}} \equiv \frac{\langle n_{\text{H}}^2 \rangle}{\langle n_{\text{H}} \rangle^2}$ is the clumping factor of ionized gas, $\alpha_B(T_0)$ is the case B hydrogen recombination coefficient for an IGM temperature of T_0 , and X and $Y = 1 - X$ are, respectively, the primordial hydrogen and helium abundances. The appropriate value of the clumping factor of ionized gas is uncertain and varies based on definition and method (see Robertson et al. 2013, and references therein). We therefore follow the literature and choose a value of $C_{\text{HII}} = 3$ (Kuhlen & Faucher-Giguère 2012; Schultz et al. 2014). We also follow previous work in adopting the commonly assumed values of $T_0 = 2 \times 10^4$ K, $X = 0.76$ and $Y = 0.24$ (Kuhlen & Faucher-Giguère 2012; Schultz et al. 2014). The primordial helium and hydrogen abundances are consistent with both CMB measurements (Komatsu et al. 2011) and estimates from low-metallicity extragalactic regions (Izotov & Thuan 2004; Steigman 2007). The assumed IGM temperature is appropriate for ionized gas at the mean density during the epoch of reionization (Hui & Haiman 2003).

The production rate of ionizing photons, \dot{n}_{ion} , is given by the equation:

$$\dot{n}_{\text{ion}} = f_{\text{esc}} \int_{M_{\text{lim}}}^{\infty} \phi(M_{UV})\gamma_{\text{ion}}(M_{UV}) dM_{UV}, \quad (10)$$

where $\phi(M_{UV})$ is the galaxy UV-luminosity function given in equation (6), $\gamma_{\text{ion}}(M_{UV})$ is a conversion factor that converts the galactic UV-luminosity to hydrogen ionizing photon luminosity, and f_{esc} represents the escape fraction of ionizing photons. We use equation 6 of Kuhlen & Faucher-Giguère (2012) that defines:

$$\gamma_{\text{ion}}(M_{UV}) \equiv 2 \times 10^{25} \text{ s}^{-1} (10^{0.4(51.63 - M_{UV})}) \zeta_{\text{ion}}, \quad (11)$$

where the second term is the galactic rest-frame UV (1500 Å) luminosity using AB magnitudes, and ζ_{ion} is a dimensionless parameter that contains all assumptions of the galaxy stellar spectrum properties, e.g. the slope of the UV continuum. We adopt the fiducial model of Kuhlen & Faucher-Giguère (2012) and set $\zeta_{\text{ion}} = 1$. The values of M_{lim} and f_{esc} are model parameters that we allow to vary in our analysis. For aMDM models where the $M_h(M_{UV})$ relation truncates prior to reaching M_{lim} , equation (10) is integrated down to the truncation magnitude in place of M_{lim} .

The most robust constraint on the epoch of reionization is the CMB Thompson scattering optical depth, τ . The CMB optical depth is an integral over the reionization history to redshift z , given by the equation:

$$\tau(z) = \int_0^z \frac{c(1+z')^2}{H(z')} Q_{\text{HII}}(z') \sigma_{\text{T}} \bar{n}_{\text{H}} (1 + \eta Y/4X) dz', \quad (12)$$

where c is the speed of light, $H(z)$ is the Hubble parameter, σ_{T} is the Thompson scattering cross-section, and

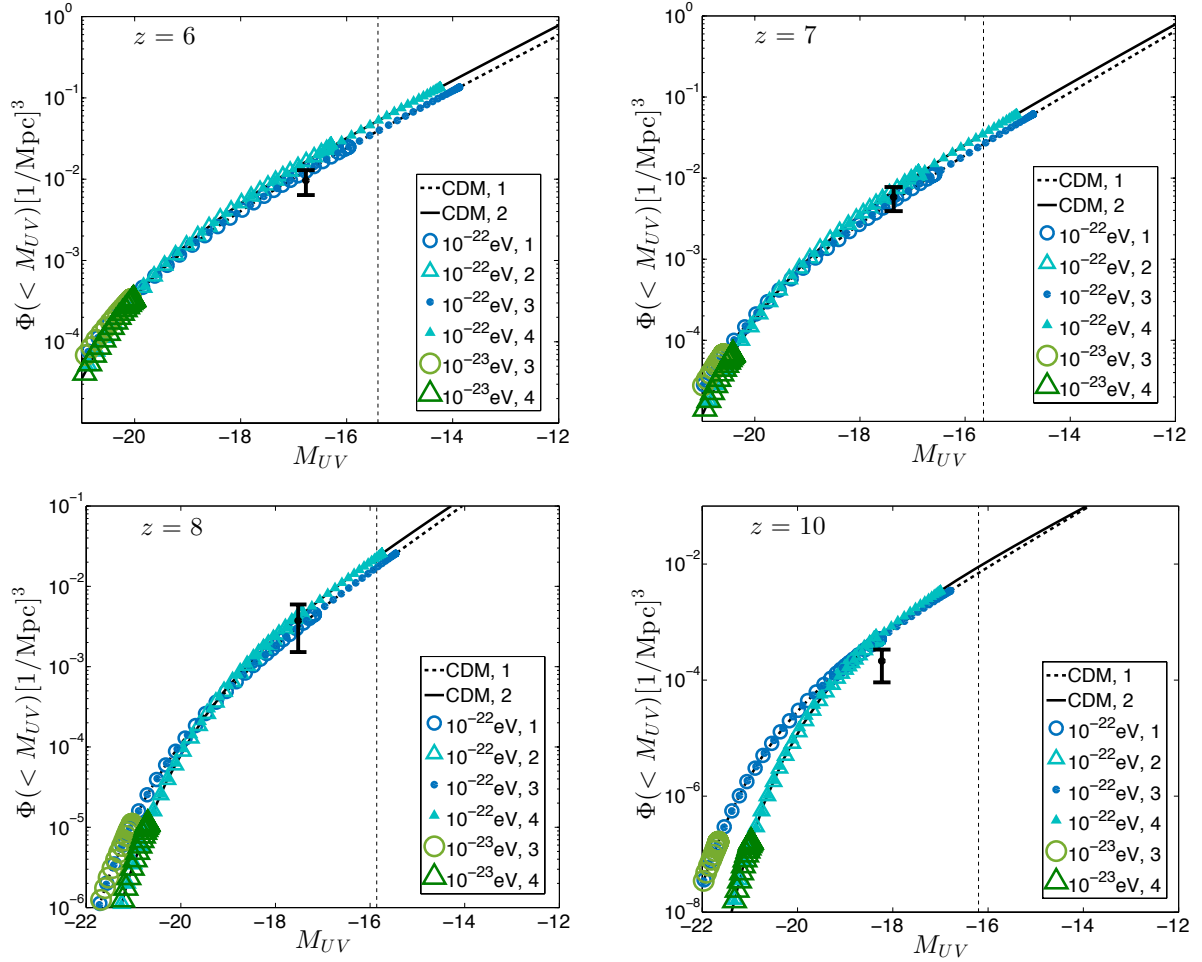


Figure 4. The cumulative luminosity functions ($z = 6, 7, 8,$ and 10) of CDM models ‘1’ (dashed black) and ‘2’ (solid black) and aMDM $m_a = 10^{-23}$ eV models ‘3’ (large green circle) and ‘4’ (large green triangle), and aMDM $m_a = 10^{-22}$ eV models ‘1’ (medium blue circle), ‘2’ (medium blue triangle), ‘3’ (small filled blue circle), ‘4’ (small filled blue triangle). The data points on each plot are the cumulative number density of galaxies in *HST* fields (Bouwens et al. 2014) summed down to the faint-end limit at each redshift. The error bars are 2σ for $z = 6, 7,$ and 8 (1σ for $z = 10$). The dashed vertical line in each panel is the absolute magnitude faint-end limit *JWST* will reach at each redshift for a survey down to an apparent magnitude of $AB = 31.5$ mag (Windhorst et al. 2006). The $m_a = 10^{-23}$ eV aMDM models truncate prior to reaching the HUDF faint-end limit, and thus this model is ruled out ($> 8\sigma$). The truncation magnitude for the $m_a = 10^{-22}$ eV models scales according to Ω_a/Ω_d , but all axion fractions of DM are consistent with HUDF constraints. The $m_a = 10^{-21}$ eV models are not shown on this plot as they are indistinguishable from CDM over the scales shown. Note: The x -axis and y -axis limits are different in each panel.

η gives the ionization state of helium. Following Kuhlen & Faucher-Giguère (2012), we assume helium is singly ionized ($\eta = 1$) at $z > 4$ and doubly ionized ($\eta = 2$) at $z \leq 4$.

6 RESULTS

6.1 aMDM cumulative luminosity functions

The aMDM cumulative luminosity functions of the $m_a = 10^{-21}$ eV, 10^{-22} eV, and 10^{-23} eV models for the redshifts $z = 6, 7, 8, 10,$ and 13 are shown in Figs 4 and 5. For each axion mass model, we allow four model pa-

rameters to vary: the Schechter function fit, the axion fraction of DM (Ω_a/Ω_d), the escape fraction of ionizing photons (f_{esc}), and the minimum UV magnitude (M_{lim}). Table 1 lists the model label and set of parameter values used in each model. The model number (‘1’ to ‘4’) refers to the Schechter function fit and the axion fraction of DM, while the letter in the model label (‘a–d’) refers to the model reionization parameters: f_{esc} and M_{lim} . We will ignore the letter in the model label in this section as the two model parameters it references do not affect the cumulative luminosity functions for the range of magnitudes shown.

The CDM cumulative luminosity functions at each

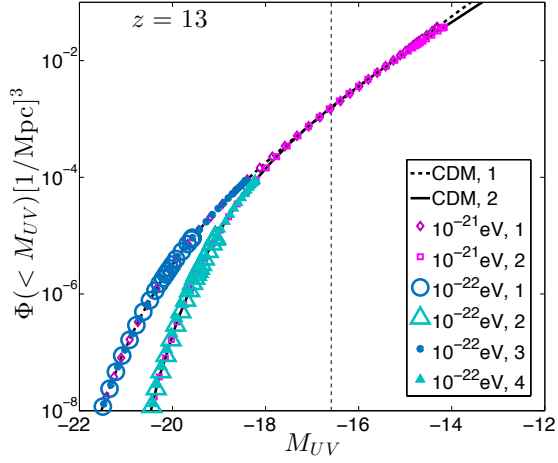


Figure 5. The cumulative luminosity functions ($z = 13$) of CDM models ‘1’ (dashed black) and ‘2’ (solid black) and aMDM $m_a = 10^{-21}$ eV models ‘1’ (small purple diamond) and ‘2’ (small purple square), and aMDM $m_a = 10^{-22}$ eV models ‘1’ (medium blue circle), ‘2’ (medium blue triangle), ‘3’ (small filled blue circle), ‘4’ (small filled blue triangle). The $m_a = 10^{-23}$ eV models are not shown as their maximum cumulative luminosity value fall below the y -axis minimum. The dashed vertical line is the absolute magnitude faint-end limit $JWST$ will reach for a survey down to an apparent magnitude of $AB = 31.5$ mag (Windhorst et al. 2006). $JWST$ observations with this sensitivity will be able to constrain $m_a = 10^{-22}$ eV models, but will be unable to distinguish $m_a = 10^{-21}$ eV models from CDM.

redshift are also plotted in Figs. 4 and 5. The two Schechter function parameterizations used in our analysis produce similar CDM cumulative luminosity functions (CDM models ‘1’ and ‘2’) below $z \leq 8$, but differ at the bright end for $z > 8$ (as seen in Fig. 5). We explore how these differences in the UV-luminosity function can produce large differences in the reionization history in the next section.

The cumulative luminosity functions for all $m_a = 10^{-23}$ eV models truncate prior to reaching the Hubble Ultra Deep Field (HUDF) faint-end limit at all redshifts greater than $z = 6$. When this axion is 100 per cent of the DM the cumulative luminosity functions truncate where there are no low mass haloes to host galaxies with fainter magnitudes in the redshift range $z = 6$ – 13 (models 1 and 2 therefore do not appear in the plots), while some haloes are produced when this axion is 50 per cent of the DM (models 3 and 4). The DM HMFs of models ‘3’ and ‘4’ at $z = 6$ are suppressed at the low-mass end such that, while there are low-mass haloes below the mass associated with the cumulative luminosity function truncation magnitude, there is not a sufficient number of haloes to host the inferred number of faint galaxies.

The truncation magnitude will vary somewhat depending on the Schechter function model, but in the

Table 1. Axion mixed DM models

Model	Schechter fit	Ω_a/Ω_d	f_{esc}	M_{lim}
1a	Bouwens	1.0	0.2	-13
1b	Bouwens	1.0	0.2	-10
1c	Bouwens	1.0	0.5	-13
1d	Bouwens	1.0	0.5	-10
2a	Kuhlen	1.0	0.2	-13
2b	Kuhlen	1.0	0.2	-10
2c	Kuhlen	1.0	0.5	-13
2d	Kuhlen	1.0	0.5	-10
3a	Bouwens	0.5	0.2	-13
3b	Bouwens	0.5	0.2	-10
3c	Bouwens	0.5	0.5	-13
3d	Bouwens	0.5	0.5	-10
4a	Kuhlen	0.5	0.2	-13
4b	Kuhlen	0.5	0.2	-10
4c	Kuhlen	0.5	0.5	-13
4d	Kuhlen	0.5	0.5	-10

Column 1: Model label, Column 2: Schechter function parameter set, Column 3: axion fraction of DM, Column 4: escape fraction of ionizing photons, Column 5: limiting magnitude of UV-luminosity function. The alphabetic order of the letters in column 1 signifies a progression in the reionization parameter assumptions from most conservative to least conservative, such that ‘a’ indicates the most conservative reionization assumptions (i.e. the smallest escape fraction and brightest limiting magnitude) and ‘d’ corresponds to the least conservative assumptions. CDM models use only the 1a–1d and 2a–2d labels.

models we consider the variation is small and is unable to bring $m_a = 10^{-23}$ eV into agreement with the data. The cumulative luminosity function (y -axis) value at truncation in each panel of Fig. 4 gives the total abundance of galaxies at that redshift and must reach the HUDF data point in order to account for the currently observed number count of galaxies. Falling below the data point indicates the model predicts fewer galaxies than are already observed. We use the error bars in Fig. 4 to calculate the χ^2 (following the method of Schultz et al. 2014) to quantify disagreement of the $m_a = 10^{-23}$ eV aMDM models with HUDF data. The HUDF data rules out ULAs with $m_a \leq 10^{-23}$ eV from contributing more than half of the total DM at greater than 8σ .

The $m_a = 10^{-22}$ eV and $m_a = 10^{-21}$ eV aMDM model cumulative luminosity functions, for all axion fractions of DM, are indistinguishable from CDM down to magnitudes fainter than the HUDF faint-end limit for the redshifts $z = 6$ – 10 . The $m_a = 10^{-21}$ eV aMDM

models are not shown for $z = 6\text{--}10$ as they are consistent with CDM for all magnitudes plotted at these redshifts. We show the cumulative luminosity functions of $m_a = 10^{-21}$ eV models ‘1’ and ‘2’ at $z = 13$ in Fig. 5. The cumulative luminosity functions truncate at a magnitude of $M_{UV} \approx -14$ distinguishing this mass from CDM at high- z .

The $m_a = 10^{-22}$ eV cumulative luminosity functions for models ‘1’ and ‘2’ (where ULAs account for all of the DM) truncate at a magnitude only slightly fainter than the HUDF limit for $z = 8$ and 10. The dashed vertical lines in Fig. 4 show the faint-end limit of a *JWST* ‘deep field’ survey for the redshift range $z = 6\text{--}13$ down to an apparent magnitude of $AB = 31.5$ mag. At this limiting magnitude it is not possible to distinguish CDM from $m_a = 10^{-21}$ eV at $z = 13$. The ULA model with $m_a = 10^{-22}$, however, predicts that no galaxies with limiting magnitude $M_{UV} \approx -16$ should be seen at high- z , and therefore a non-observation by *JWST* would provide evidence that the DM could be composed of such a ULA. A non-observation by *JWST* at $M_{UV} \approx -16$ does not rule out CDM or $m_a = 10^{-21}$ models, but would require a physical explanation for suppression of galaxy formation at that magnitude. On the other hand, if *JWST* does observe galaxies with limiting magnitude $M_{UV} \approx -16$ at high- z this would rule out $m_a = 10^{-22}$ eV as a dominant component of the DM.

6.2 aMDM reionization history

The reionization histories of the aMDM and CDM models, $Q_{\text{HII}}(z)$, are shown in the left- and right-hand panels of Fig. 6. The evolution of $Q_{\text{HII}}(z)$ in a CDM cosmology, shown in the left-hand panel of Fig. 6, depends strongly on the Schechter function model, the assumed value of the escape fraction of ionizing photons, f_{esc} , and the minimum UV magnitude, M_{lim} . The extreme reionization history of CDM model ‘1d’ (dashed pink curve) is likely to be unphysical, but is included in Fig. 6 in order to illustrate the full range of reionization histories produced by case ‘d’ reionization models and to facilitate comparison with aMDM model ‘4d’ results.

The $m_a = 10^{-23}$ eV aMDM models with axions comprising 100 per cent or 50 per cent of the DM are unable to reionize the universe by $z = 5$ in the wide range of reionization models we consider, as shown by the blue shaded region of the left-hand panel of Fig. 6. Observations of the Gunn–Peterson trough in quasar spectra at $z > 6$ (Fan et al. 2006) and transmission in the Ly α forest for $z < 6$ (Becker et al. 2001; Djorgovski et al. 2001; Fan et al. 2001) suggests the epoch of reionization ends at $z \sim 6$ ($Q_{\text{HII}}(z \sim 6) > 0.99$). These constraints on the neutral fraction of hydrogen at the end of reionization rely on detailed modelling of both the IGM and ionizing sources making their accuracy (and therefore the exact end of reionization) the subject of debate (Becker, Rauch & Sargent 2007; Furlanetto & Mesinger 2009; Mesinger 2010; McGreer, Mesinger & Fan 2011;

Robertson et al. 2013). McGreer, Mesinger & Fan (2011) use the covering fraction of ‘dark’ pixels in quasar spectra to obtain the more conservative constraints of $Q_{\text{HII}}(z = 5.5) > 0.8$ and $Q_{\text{HII}}(z = 6) > 0.5$ on the end of reionization. The most extreme $m_a = 10^{-23}$ eV model ‘4d’ value of $Q_{\text{HII}}(z = 6) = 0.19$ is inconsistent with even these more conservative constraints. The reionization history therefore rules out $m_a = 10^{-23}$ eV from contributing more than half of the DM, consistent with the constraints of Section 6.1.

The $m_a = 10^{-21}$ eV aMDM models have a range of reionization histories, depicted by the dark purple (rightmost) shaded region in the right-hand panel of Fig. 6, depending on the assumed value of the escape fraction and Schechter function fit. Each case completes reionization by $z = 6$. The reionization histories of the most conservative reionization model, ‘1a’, for $m_a = 10^{-21}$ eV, represented by the leftmost edge of the dark purple shaded region, and CDM (orange, solid curve) are similar for $z < 8$. The early reionization history ($Q_{\text{HII}}(z > 8)$), is more extended for CDM. The range of possible reionization histories is less varied for the $m_a = 10^{-21}$ eV aMDM models than CDM, as seen in the comparison of the right edge of the purple (right) shaded region with the pink (dashed) curve in Fig. 6 (right-hand panel). This is due to the delay in the build-up of small-mass haloes in an $m_a = 10^{-21}$ eV aMDM cosmology compared to CDM such that the $m_a = 10^{-21}$ eV aMDM early reionization history is less affected by changes in reionization model assumptions. We see that it is possible for the reionization history of the Universe to distinguish CDM from $m_a = 10^{-21}$ eV under certain assumptions. We will return to this question in Section 6.4.

The reionization histories of the $m_a = 10^{-22}$ eV aMDM models represented by the blue shaded (leftmost) region in Fig. 6 complete reionization by $z = 6$ depending on the assumed value of the escape fraction, Schechter function fit, and the axion fraction of dark matter. A larger escape fraction ($f_{\text{esc}} = 0.5$) or a smaller axion fraction of DM ($\Omega_a/\Omega_d = 0.5$) is required to complete reionization by $z = 6$. All models complete reionization by $z = 5.5$ and are consistent with the more conservative Ly α constraints of McGreer, Mesinger & Fan (2011). The $m_a = 10^{-22}$ eV aMDM model reionization histories are more abbreviated compared to CDM due to the relative delay in small-mass galaxy formation. In most cases for the $m_a = 10^{-22}$ eV aMDM models, changing the limiting magnitude from $M_{\text{lim}} = -10$ to -13 produces little to no change in $Q_{\text{HII}}(z)$ as both limits fall below the magnitude where the $M_h(M_{UV})$ relation truncates. Due to the weaker dependence on model assumptions reionization is able to constrain $m_a = 10^{-22}$ eV rather well.

6.3 CMB optical depth

The left- and right-hand panels of Fig. 7 show the predictions for the CMB optical depth, τ , for the aMDM

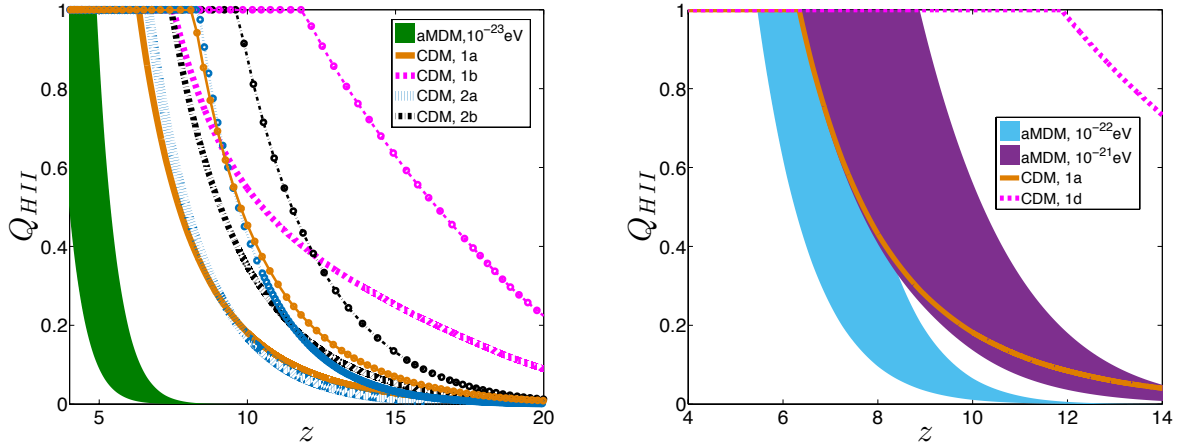


Figure 6. The reionization histories of the aMDM and CDM models. Left-hand panel: CDM ‘1a’ (thick, solid orange), CDM ‘1b’ (thick, dashed pink); CDM ‘1c’ (thin, solid orange /circle markers); CDM ‘1d’ (thin, dashed pink/circle markers); CDM ‘2a’ (thick, dotted blue); CDM ‘2b’ (thick, dash–dotted black); CDM ‘2c’ (thin, dotted blue/circle markers); CDM ‘2d’ (thin, dash–dotted black/circle markers). The full range of $m_a = 10^{-23}$ eV reionization histories are represented by the green patch. The $m_a = 10^{-23}$ eV aMDM models are unable to reionize the universe by $z = 5$. Right-hand panel: the full range of $m_a = 10^{-22}$ eV reionization histories are represented by the light blue patch. CDM models ‘1a’ and ‘1d’ are shown for reference (x -axis has a different scale in each panel). The $m_a = 10^{-22}$ eV aMDM model reionization histories complete reionization by $z = 6$ depending on the assumed reionization parameters. All models complete reionisation by $z = 5.5$. The reionization histories of the $m_a = 10^{-21}$ eV aMDM models complete reionization by $z = 6$.

and CDM models. The CMB optical depth is plotted cumulatively as a function of redshift. The predicted full-integrated value of τ for each model can be taken from the high-redshift end of the plot for comparison with CMB measurements. The grey (horizontal) bands in both figures show the 68 per cent (1σ) and 95.45 per cent (2σ) confidence levels around the maximum likelihood value of $\tau = 0.0891$ from the recent *Planck*+*WMAP* analysis by Spergel, Flauger & Hlozek (2013). We will quote results for the 99.73 per cent (3σ) confidence level where applicable; however, this region is not plotted in either figure for simplicity.

The CDM and $m_a = 10^{-23}$ eV aMDM model predictions for τ are shown in the left-hand panel of Fig. 7. The τ values predicted for the CDM models depend strongly on the model’s reionization assumptions. The more conservative assumptions of CDM models ‘1a’ and ‘1b’ give results that are consistent with *Planck*+*WMAP* constraints at the 95.5 per cent confidence level. Only CDM model ‘1d’ is ruled out at more than 99.99 per cent confidence and is included here to contrast against the aMDM maximal reionization models.

The green (lower) shaded patch in the left-hand panel of Fig. 7 shows the full range of possible CMB optical depth values for the $m_a = 10^{-23}$ eV aMDM model. The upper bound (given by model ‘4d’) is excluded at greater than 99.73 per cent confidence. The slow build-up of small galaxies in the $m_a = 10^{-23}$ eV aMDM models, which produces a delayed reionization

history in this cosmology, prohibits the model from reproducing a value of τ consistent with *Planck*+*WMAP* constraints. We see yet again that, taking into account a wide range of models for reionization to bracket our systematic uncertainty, $m_a = 10^{-23}$ eV contributing more than 50 per cent of the DM is ruled out, consistent with the constraints from Sections 6.1 and 6.2.

The CMB optical depth predictions for the $m_a = 10^{-21}$ eV and the $m_a = 10^{-22}$ eV aMDM models are shown in the right-hand panel of Fig. 7. The $m_a = 10^{-22}$ eV aMDM model predictions for τ are depicted by the four blue curves shown in Fig. 7. The predicted τ values of models ‘1a’, ‘1b’, ‘2a’, ‘2b’ are excluded by *Planck*+*WMAP* constraints at the 99.73 per cent confidence level. Therefore, in conservative models of reionization, $m_a = 10^{-22}$ eV is excluded from being all of the DM at more than 3σ . The other $m_a = 10^{-22}$ eV aMDM model predictions for τ , however, are well within the 99.73 per cent confidence region, and the τ values of models ‘3c’, ‘3d’, ‘4c’, and ‘4d’ are within the 95.5 per cent confidence region. In the more extreme models of reionization, $m_a = 10^{-22}$ eV is allowed to contribute up to half of the DM while remaining consistent with the observed value of τ at 2σ .

The Schechter function fit and the value of limiting magnitude have little or no effect on the predicted τ values for all axion fractions of DM of the $m_a = 10^{-22}$ eV aMDM model. The assumed value of the escape fraction of ionizing photons is the only reionization parameter that strongly affects the predicted value of τ for

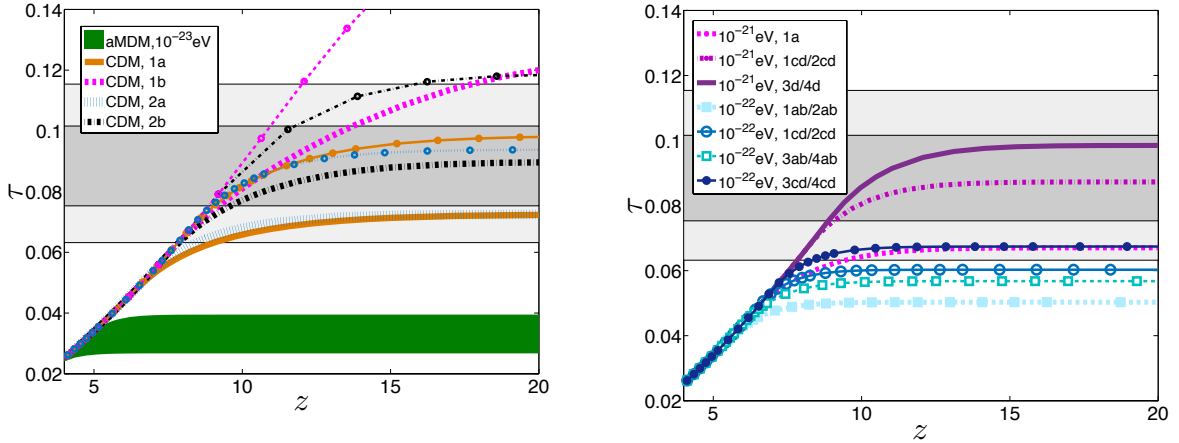


Figure 7. The CMB optical depth, τ , for the aMDM and CDM models. The grey (horizontal) bands in both panels are *Planck*+*WMAP* 68 per cent (1σ , dark grey) and 95.45 per cent (2σ , light grey) confidence levels. Left-hand panel: CDM ‘1a’ (thick, solid orange); CDM ‘1b’ (thick, dashed pink); CDM ‘1c’ (thin, solid orange/circle markers); CDM ‘1d’ (thin, dashed pink/circle markers); CDM ‘2a’ (thick, dotted blue); CDM ‘2b’ (thick, dash-dotted black); CDM ‘2c’ (thin, dotted blue/circle markers); CDM ‘2d’ (thin, dash-dotted black/circle markers). The full range of $m_a = 10^{-23}$ eV aMDM model predictions for τ are represented by the shaded green patch. The $m_a = 10^{-23}$ eV aMDM model is excluded at greater than 99.99 per cent confidence. Right-hand panel: $m_a = 10^{-22}$ eV models ‘1ab/2ab’ (dashed, light blue curve/filled square markers); $m_a = 10^{-22}$ eV models ‘1cd/2cd’ (solid, blue/open circle); $m_a = 10^{-22}$ eV models ‘3ab/4ab’ (dashed, cyan/open square); $m_a = 10^{-22}$ eV models ‘3cd/4cd’ (solid, dark blue/filled circle); $m_a = 10^{-21}$ eV ‘1a’ (dashed magenta); $m_a = 10^{-21}$ eV models ‘1cd/2cd’ (dash-dotted purple); $m_a = 10^{-21}$ eV models ‘1cd/2cd’ (solid dark purple). The $m_a = 10^{-22}$ eV aMDM model predictions for τ (right-hand panel) is in tension with *Planck*+*WMAP* constraints. Only the $m_a = 10^{-22}$ eV aMDM model with axions contributing only 50 per cent of the DM and with the most extreme reionization assumptions is consistent at 95.45 per cent (2σ) confidence. Less conservative models with larger DM fraction in axions are in more tension. The $m_a = 10^{-21}$ eV aMDM model τ predictions are all consistent with *Planck*+*WMAP* constraints and depend strongly on the reionization parameter assumptions.

this aMDM model. Tighter constraints on the observed value of τ (with the same maximum likelihood value) by future CMB experiments could place considerable tension on this model.

The upper and lower bounds of the $m_a = 10^{-21}$ eV aMDM model predictions for τ are, respectively, represented by the solid, dark purple curves (models ‘3d’ and ‘4d’) and dashed magenta curves (model ‘1a’) in the right-hand panel of Fig. 7. CMB optical depth values predicted for all other $m_a = 10^{-21}$ eV aMDM models are within these two bounding curves and are consistent with *Planck*+*WMAP* constraints for all axion fractions of DM and reionization model assumptions. The τ prediction of models ‘1c’, ‘1d’, ‘2c’, and ‘2d’ that are closest to the maximum likelihood value of *Planck*+*WMAP* are represented by the dashed magenta curve in the right-hand panel of Fig. 7.

The reionization parameter assumptions have a larger effect on the $m_a = 10^{-21}$ eV aMDM model than the other aMDM models. The most important reionization parameter is the value of the escape fraction. The subsequent importance of the limiting magnitude and choice of Schechter function depends on the axion fraction of DM and the value of the escape fraction. For example, there is a small spread in the predicted value of τ for models ‘1a’, ‘1b’, ‘2a’, and ‘2b’, while the models ‘1c’, ‘1d’, ‘2c’, and ‘2d’ are all very similar. For axion

fractions of DM $\Omega_a/\Omega_d = 0.5$ (models ‘3’ and ‘4’), the choice of limiting magnitude effects the predicted value of τ , but the Schechter function fit does not, i.e. the τ values of models ‘3d’ and ‘4d’ are similar and greater than the similar τ values of models ‘3c’ and ‘4c’ (not shown in Fig. 7).

6.4 Measuring the duration of reionization

Future small-scale CMB polarization measurements, such as the proposed Advanced ACTPol (AdvACT) experiment, aim to constrain the epoch of reionization through an accurate measurement of the kinematic Sunyaev–Zel’dovich (kSZ) effect (Sunyaev & Zel’dovich 1980) by breaking degeneracies between primary and secondary contributions to temperature anisotropies (Calabrese et al. 2014). The AdvACT experiment measurement of the patchy kSZ power spectrum amplitude and multipole shape could constrain the duration of reionization ($\delta z_{\text{re}} = z_f(Q_{\text{HII}} = 0.75) - z_i(Q_{\text{HII}} = 0.25)$) and the median redshift of reionization $z_{\text{re,med}} = z(Q_{\text{HII}} = 0.5)$ respectively, to an uncertainty of $\sigma(\delta z_{\text{re}}) = 0.2$ and $\sigma(z_{\text{re,med}}) = 1.1$.

We explore the ability of the AdvACT experiment to distinguish between the $m_a = 10^{-21}$ eV aMDM and CDM models by examining the AdvACT constraints

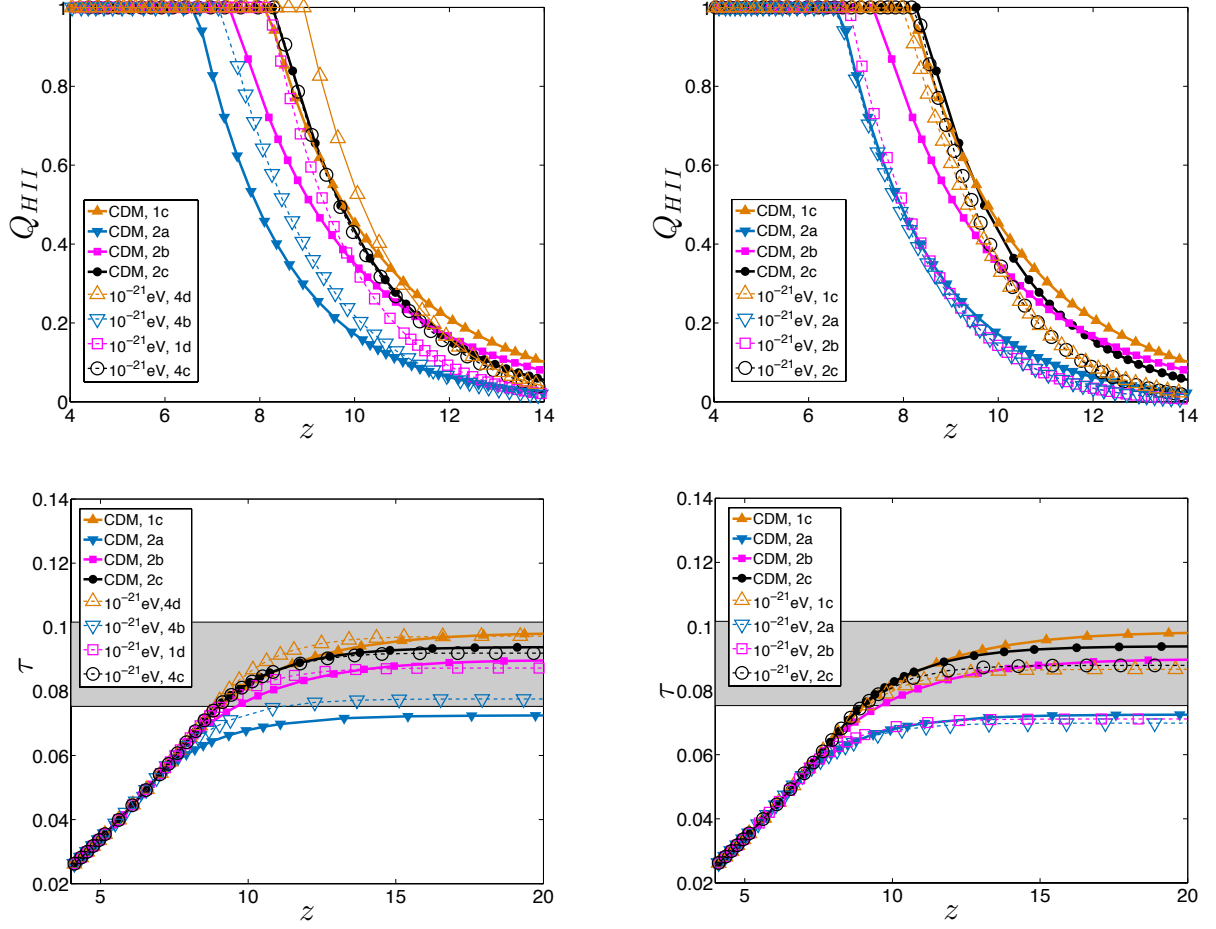


Figure 8. The reionization histories (top row) and CMB optical depth values (bottom row) of two sets of four $m_a = 10^{-21}$ eV aMDM models compared to a set of four CDM models {‘1c’ (solid orange curve/filled triangle marker), ‘2a’ (solid blue/upside-down, filled triangle), ‘2b’ (solid pink/filled square), ‘2c’ (solid black/filled circle)}. Left-hand panels: the first aMDM set { ‘4d’ (dashed orange/open triangle), ‘4b’ (dashed blue/open upside-down triangle), ‘1d’ (dashed pink/open square), ‘4c’ (dashed black/open circle)} is selected τ consistent at 1σ (grey band) with *Planck*+*WMAP* value and provide a close match to each CDM model’s τ prediction. Right-hand panels: { ‘1c’ (dashed orange/open triangle), ‘2a’ (dashed blue/open upside-down triangle), ‘2b’ (dashed pink/open square), ‘2c’ (dashed black/open circle)} have the same reionization assumptions as the four CDM models. Models that are differentiable from CDM by the duration of reionization (according to AdvACT constraints): ‘Set 1’ - (‘1d’ and ‘4d’) and ‘Set 2’ - (‘1c’, ‘2b’, and ‘2c’)

on a set of reionization models for CDM and aMDM. We chose four CDM models that span a range of reionization assumptions and predict the corresponding τ values that are consistent with *Planck*+*WMAP* at 2σ , namely ‘1c’, ‘2a’, ‘2b’, and ‘2c’. We compare two sets of $m_a = 10^{-21}$ eV aMDM models to this set of CDM models. The first set (‘4d’, ‘4b’, ‘1d’, and ‘4c’), shown in the left-hand panels of Fig. 8, is selected to have a predicted value of τ that is consistent with *Planck*+*WMAP* at 1σ and as close a match to the selected CDM model’s τ prediction as possible. The second set, shown in the right-hand panels of Fig. 8, is selected to have the same reionization assumptions as the four CDM models and an axion fraction of DM of $\Omega_a/\Omega_d = 1.0$. The dura-

tion of reionization, the median redshift of reionization, and the discriminating power of AdvACT to separate comparable models are listed in Table 2.

Two of the four models in the first set (‘1d’ and ‘4d’), shown in the left-hand column of Fig. 8, have a duration of reionization that is differentiable from their CDM counterpart at 4σ , even though their median redshift of reionization is within 1σ of CDM and they share a similar prediction for τ . The more extreme ‘d’ models of reionization, with large escape fraction and limiting magnitude, are necessary for $m_a = 10^{-21}$ eV to match τ values of less extreme CDM models. Yet these models complete reionization more rapidly than their CDM counterparts and can thus be distinguished AdvACT.

Table 2. AdvACT constraints on $m_a = 10^{-21}$ eV aMDM models

aMDM model	δz_{re}	$z_{\text{re,med}}$	CDM model	δz_{re}	$z_{\text{re,med}}$	CL $\{z_{\text{re}}\}$	CL $\{\delta z_{\text{re}}\}$
4d	1.86	10.15	Model 1c	2.73	9.77	27.0 per cent	99.9989 per cent
4b	1.99	8.52	Model 2a	2.08	7.93	40.8 per cent	38.3 per cent
1d	1.80	9.37	Model 2b	2.72	9.09	20.1 per cent	99.9996 per cent
4c	2.10	9.68	Model 2c	2.17	9.70	1.5 per cent	31.1 per cent
1c	1.90	9.35	Model 1c	2.73	9.77	29.7 per cent	99.997 per cent
2a	1.95	7.88	Model 2a	2.08	7.93	3.6 per cent	51.6 per cent
2b	1.80	8.01	Model 2b	2.72	9.09	67.4 per cent	99.997 per cent
2c	1.73	9.47	Model 2c	2.17	9.70	16.6 per cent	97.2 per cent

Column 1: aMDM model label, Column 2: aMDM model duration of reionization ($\delta z_{\text{re}} = z_f(Q_{\text{HII}} = 0.75) - z_i(Q = 0.25)$), Column 3: aMDM model median redshift of reionization $z_{\text{re,med}} = z(Q_{\text{HII}} = 0.5)$, Column 4: CDM model label, Column 5: CDM model duration of reionization, Column 6: CDM model median redshift of reionization, Column 7: confidence level of AdvACT ability to differentiate between aMDM and CDM model's median redshift of reionization, Column 8: confidence level of AdvACT ability to differentiate between aMDM and CDM model's duration of reionization. The set of four aMDM models above the horizontal line make up 'Set 1' and the four aMDM models below the horizontal line make up 'Set 2'. The aMDM models that are distinguishable from CDM based on AdvACT constraints on the duration of reionization: 'Set 1' - ('Model 1d' and 'Model 4d'), 'Set 2' - ('Model 1c', 'Model 2b', and 'Model 2c').

From the second set, three of the four $m_a = 10^{-21}$ eV aMDM models ('1c', '2b', and '2c'), have a reionization duration that is distinct from CDM at greater than 2σ under the same reionization assumptions. With the exception of the most conservative 'a' model of reionization, the large axion fraction of DM leads the axion models to different values of τ from CDM, though all easily within 2σ of the *Planck*+*WMAP* constraint. Reionization again completes more rapidly with axion DM than CDM, which will allow AdvACT to constrain aMDM models with large fractions of axion DM.

Taken together, the results of these two sets indicate that reionization histories for a subset of $m_a = 10^{-21}$ eV aMDM models can be distinguished from CDM by AdvACT constraints. As discussed in Section 6.2, the $m_a = 10^{-21}$ eV aMDM and CDM models with more conservative reionization assumptions have similar reionization histories, while the CDM model has a more varied response to more extreme reionization assumptions. The median redshift of reionization, $z_{\text{re,med}}$, for the CDM and aMDM models (listed in Table 2) provides a dividing line for CDM and aMDM models that can be differentiated by AdvACT and those that cannot. The aMDM and CDM models where both models have a median redshift of reionisation of $z_{\text{re,med}} < 8.6$ are indistinguishable by AdvACT constraints. These aMDM and CDM models have more conservative reionization assumptions that give similar reionization histories, as illustrated by the aMDM models '4b' and '2a' compared with CDM model '2a' represented by the blue curves in Fig. 8. If both aMDM and CDM models have a median redshift of reionization of $z_{\text{re,med}} > 8.6$ they will have a duration of reionization that is differentiable by AdvACT constraints, if the aMDM model does not have the same reionization assumptions as the CDM model and an axion fraction of DM of $\Omega_a/\Omega_d = 0.5$. The black

curves in Fig. 8 illustrate this last point. The aMDM model '4c' has an axion fraction of DM of $\Omega_a/\Omega_d = 0.5$ and has a reionization history that is indistinguishable from CDM model '2c' as shown by the black curves in the left-hand panels of Fig. 8. The aMDM model '2c' has the same reionization assumptions as model '4c' and the CDM model '2c', but with an axion fraction of DM of $\Omega_a/\Omega_d = 1.0$ it has reionization history that is differentiable from CDM model '2c' as shown by the black curves in the right-hand panels of Fig. 8.

Complementary data and analyses that could constrain the escape fraction of ionizing photons, tighten the constraints on τ , and place either theoretical or observational constraints on the limiting magnitude of the UV-luminosity function could improve on the range of $m_a = 10^{-21}$ eV aMDM and CDM models that can be ruled out by future CMB measurements. The proposed AdvACT experiment could improve on constraints on reionization duration, median reionization redshift, and τ value by extending the temperature fluctuation multipole space down to $l = 10$.

7 SUMMARY AND DISCUSSION

We have used the model of Marsh & Silk (2013) for the HMF of ultralight aMDM (which appears broadly consistent with the simulations of Schive, Chiueh & Broadhurst 2014) to place constraints on the axion mass. To do this, we used the predicted high- z UV-luminosity function compared to that derived from deep imaging with the *HST* together with the predicted reionization history of the universe, via the optical depth, τ , compared to the value derived from the CMB. For simplicity, we have considered only models where axions comprise either all or half of the total DM. We assume that galaxies are only contributor to reionization. AGN feedback could possibly loosen some constraints. Such a model,

however, is severely contained by the diffuse X-ray background (Dijkstra, Haiman & Loeb 2004).

We have found that both the UV-luminosity function and the optical depth consistently forbid $m_a = 10^{-23}$ eV from contributing a large fraction of the DM. This appears to exclude the possibility to search for ULAs via pulsar timing experiments as proposed by Khmel'nitsky & Rubakov (2014). We have found that $m_a = 10^{-23}$ eV cannot produce enough galaxies of the required magnitude at high- z to be consistent with HUDF. Under a wide range of limiting magnitudes and escape fractions, allowing for a large uncertainty in the model for reionization, $m_a = 10^{-23}$ eV fails to reionize the universe by $z = 6$ and is inconsistent with the measured value of τ at $> 3\sigma$. In terms of DM fraction with $m_a = 10^{-23}$ eV, we have ruled out both 100 and 50 per cent at greater than 8σ . The strength of the constraints suggests that a more detailed study varying the fraction of DM in axions over a wider range will be able to limit the fraction still further at this mass. By simple extrapolation the entire ULA mass range 10^{-32} eV $\lesssim m_a \lesssim 10^{-23}$ eV is excluded, by an order of magnitude, for $\Omega_a/\Omega_d \gtrsim 0.5$ fraction of the DM.⁷

With $m_a = 10^{-22}$ eV it is just possible to produce enough high- z galaxies to be consistent with HUDF. However, under conservative assumptions for the model of reionization, $m_a = 10^{-22}$ eV is in tension with the measured value of τ at 3σ if the DM is entirely composed of axions. It is interesting to note that this encompasses the best-fitting value of $m_a = 8.1 \times 10^{-23}$ eV of Schive, Chiueh & Broadhurst (2014) required to account for a core in Fornax (see also Schive et al. 2014b). This is a major result of this paper as it puts an important part of axion parameter space, which is related to the solution of the small-scale problems, under pressure. The tension from τ is reduced to 2σ if the axion is only 50 per cent of the DM, but then core formation is likely spoiled (Marsh & Silk 2013). At high redshift, the central overdensity of axion DM haloes is decreased (Schive, Chiueh & Broadhurst 2014) compared to pure CDM haloes and the shallower potential well of the cored DM halo may impact galaxy formation in the early universe. While beyond the scope of this paper, a full investigation of the role of cored DM haloes on the star formation history, feedback efficiency, and the escape fraction of ionizing photons would provide valuable insight into galaxy formation in an aMDM cosmology. More detailed studies are needed in this area to determine whether ULAs can resolve the cusp-core problem while being consistent with the reionization history of the universe.

We have found that $m_a = 10^{-21}$ eV is consistent with the high- z UV-luminosity function and the reionization history of the universe under a wide range of models for abundance matching and reionization,

and with current observations is indistinguishable from CDM.

Can we push constraints on m_a further, and what are the observational and theoretical motivations for doing so?

A tensor-mode interpretation of primordial degree scale CMB B -mode polarization, which may have been observed by BICEP2 (Ade et al. 2014), forbids the entire range of 10^{-28} eV $\lesssim m_a \lesssim 10^{-18}$ eV from contributing any significant amount of the DM (Marsh et al. 2014b).⁸ Any evidence for the existence of a ULA in this mass range would therefore be a signal of non-trivial axion dynamics during or after inflation (e.g. Conlon et al. 2008), or a non-tensor source of B -modes (e.g. Pospelov et al. 2009). Furthermore, a range of axion masses 10^{-19} eV $\lesssim m_a \lesssim 10^{-18}$ eV is potentially ruled out from observations of spinning supermassive black holes, due to the super-radiant instability that would otherwise be present (Arvanitaki & Dubovsky 2011; Pani et al. 2012, Pani, private communication). Improving cosmological constraints on m_a by an order of magnitude or more can thus close a remaining gap in ULA parameter space, confirm or refute the role of axions in resolving the small-scale crises of CDM, and be of relevance to inflationary model building.

With $m_a = 10^{-22}$ eV the UV-luminosity function has no support for $M_{UV} \gtrsim -17$ at $z \geq 10$. The planned deep field measurement of the luminosity function by *JWST*, which we forecast to reach $M_{UV} \approx -16$ at $z \geq 10$, could therefore easily rule out, or find evidence for, this model. Furthermore, Calabrese et al. (2014) showed that near-future improvements in the measurement of CMB polarization by AdvACT will significantly improve our knowledge of the epoch, z_{re} , and duration, Δz_{re} , of reionization. Achieving $\sigma(z_{re}) = 1.1$ and $\sigma(\Delta z_{re}) = 0.2$ could distinguish $m_a = 10^{-21}$ eV from CDM, and also constrain the model of reionization. Achieving these limits from *JWST* and AdvACT on the axion contribution to DM for $m_a \gtrsim 10^{-22}$ eV would be highly significant for ULA models of structure formation (Marsh & Silk 2013; Beyer & Wetterich 2014; Schive, Chiueh & Broadhurst 2014), and for the parameter space of the ‘string axiverse’ (Arvanitaki et al. 2010). As observational probes improve it is necessary to study structure formation with axion DM further through theory and simulation, to keep up with the accuracy of the data.

ACKNOWLEDGEMENTS

We acknowledge Renée Hlozek for supplying the τ likelihood and thank Marc Kamionkowski, Russell Ryan, Pierre Sikivie, Michael Strauss, and James Taylor for

⁷ At the low-mass end, $m_a \lesssim 10^{-32}$ eV, axions behave quintessence and our constraints do not apply (Marsh et al., in preparation).

⁸ For larger masses than this it is possible for a ULA to contribute significantly to the DM density while having a small decay constant and avoiding isocurvature constraints.

useful discussions. BB, JS and RFGW acknowledge support at JHU by NSF grant OIA-1124403. DJEM's research at Perimeter Institute is supported by the Government of Canada through Industry Canada and by the Province of Ontario through the Ministry of Research and Innovation. RFGW thanks the Aspen Center for Physics and NSF Grant PHY-1066293 for hospitality during the writing of this paper. The research of JS has been supported at IAP by the ERC project 267117 (DARK) hosted by Université Pierre et Marie Curie - Paris 6.

Note added in proof: Since the submission of this manuscript the Planck 2015 polarization results have been released (Planck Collaboration XIII 2015), which give a slightly lower value of $\tau \approx 0.07 - 0.08 \pm 0.002$ (the central value depending on data set combinations). This lower value of τ no longer strongly disfavours $m_a = 10^{-22}$ eV, allowing for a ULA solution to the cusp-core problem that, as shown here, makes additional, testable, predictions for future measurements of the epoch of reionization. This is discussed further by Marsh & Pop (2015).

REFERENCES

- Aalseth C., et al., 2011, *Phys. Rev. Lett.*, 106, 131301
 Abbasi R., et al., 2012, *Phys. Rev. D*, 85, 042002
 Acharya B., Bobkov K., Kumar P., 2010, *J. High Energy Phys.*, 1011, 105
 Ackermann M., et al., 2011, *Phys. Rev. Lett.*, 107, 241302
 Ade P., et al., 2014, *Phys. Rev. Lett.*, 112, 241101
 Agnese R., et al., 2014, *Phys. Rev. Lett.*, 112, 241302
 Aguilar M., et al., 2013, *Phys. Rev. Lett.*, 110, 141102
 Akerib D., et al., 2014, *Phys. Rev. Lett.*, 112, 091303
 Amendola L., Barbieri R., 2006, *Phys. Lett. B*, 642, 192
 Amendola L., et al., 2013, *Living Rev. Relativ.*, 16, 6
 Angloher G., et al., 2014, *Eur. Phys. J. C*, 74, 3184
 Aprile E., et al., 2012, *Phys. Rev. Lett.*, 109, 181301
 Arkani-Hamed N., Motl L., Nicolis A., Vafa C., 2007, *J. High Energy Phys.*, 0706, 060
 Arvanitaki A., Dimopoulos S., Dubovsky S., Kaloper N., March-Russell J., 2010, *Phys. Rev. D*, 81, 123530
 Arvanitaki A., Dubovsky S., 2011, *Phys. Rev. D*, 83, 044026
 Asztalos S., et al., 2010, *Phys. Rev. Lett.*, 104, 041301
 Baer H., Choi K.-Y., Kim J. E., Roszkowski L., 2014, preprint (arXiv:1407.0017)
 Becker G. D., Rauch M., Sargent W. L. W., 2007, *ApJ*, 662, 72
 Becker R. H. et al., 2001, *AJ*, 122, 2850
 Belikov A. V., Hooper D., 2009, *Phys. Rev. D*, 80, 035007
 Bennett C., et al., 2013, *ApJS*, 208, 20
 Benson A. J. et al., 2013, *MNRAS*, 428, 1774
 Beringer J., et al., 2012, *Phys. Rev. D*, 86, 010001
 Beyer J., Wetterich C., 2014, *Phys. Lett. B*, 738, 418
 Blum K., D'Agnolo R. T., Lisanti M., Safdi B. R., 2014, *Phys. Lett. B*, 737, 30
 Blumenthal G. R., Faber S. M., Primack J. R., Rees M. J., 1984, *Nature*, 311, 517
 Bode P., Ostriker J. P., Turok N., 2001, *ApJ*, 556, 93
 Bond J. R., Szalay A. S., 1983, *ApJ*, 274, 443
 Bond J. R., Szalay A. S., Turner M. S., 1982, *Phys. Rev. Lett*, 48, 1636
 Bouwens R. J. et al., 2011, *ApJ*, 737, 90
 Bouwens R. J. et al., 2014, preprint (arXiv:1403.4295)
 Boylan-Kolchin M., Bullock J. S., Garrison-Kimmel S., 2014, *MNRAS*, 443, L44
 Boylan-Kolchin M., Bullock J. S., Kaplinghat M., 2011, *MNRAS*, 415, L40
 Boyle L. A., Caldwell R. R., Kamionkowski M., 2002, *Phys. Lett. B*, 545, 17
 Brockway J. W., Carlson E. D., Raffelt G. G., 1996, *Phys. Lett. B*, 383, 439
 Budker D., Graham P. W., Ledbetter M., Rajendran S., Sushkov A., 2014, *Phys. Rev. X*, 4, 021030
 Bunker A. J., Stanway E. R., Ellis R. S., McMahon R. G., 2004, *MNRAS*, 355, 374
 Calabrese E. et al., 2014, *J. Cosmol. Astropart. Phys.*, 8, 10
 Cicoli M., Goodsell M., Ringwald A., 2012, *J. High Energy Phys.*, 1210, 146
 Chiueh T., 2014, preprint (arXiv:1409.0380)
 Conlon J. P., Kallosh R., Linde A. D., Quevedo F., 2008, *J. Cosmol. Astropart. Phys.*, 0809, 011
 Davis M., Efstathiou G., Frenk C. S., White S. D. M., 1985, *ApJ*, 292, 371
 Dayal P., Mesinger A., Pacucci F., 2014, preprint (arXiv:1408.1102)
 Dijkstra M., Haiman Z., Loeb A., 2004, *ApJ*, 613, 646
 Djorgovski S. G., Castro S., Stern D., Mahabal A. A., 2001, *ApJ*, 560, L5
 Fan X. et al., 2001, *AJ*, 122, 2833
 Fan X. et al., 2006, *AJ*, 132, 117
 Fontanot F., Cristiani S., Vanzella E., 2012, *MNRAS*, 425, 1413
 Friedland A., Giannotti M., Wise M., 2013, *Phys. Rev. Lett.*, 110, 061101
 Furlanetto S. R., Mesinger A., 2009, *MNRAS*, 394, 1667
 Grifols J., Masso E., Toldra R., 1996, *Phys. Rev. Lett.*, 77, 2372
 Gunn J. E., Peterson B. A., 1965, *ApJ*, 142, 1633
 Haiman Z., Loeb A., 1998, *ApJ*, 503, 505
 Hu W., 1998, *ApJ*, 506, 485
 Hu W., Barkana R., Gruzinov A., 2000, *Phys. Rev. Lett.*, 85, 1158
 Hui L., Haiman Z., 2003, *ApJ*, 596, 9
 Izotov Y. I., Thuan T. X., 2004, *ApJ*, 602, 200
 Jungman G., Kamionkowski M., Griest K., 1996, *Phys. Rep.*, 267, 195
 Khlopov M. I., Malomed B. A., Zeldovich I. B., 1985, *MNRAS*, 215, 575
 Khmel'nitsky A., Rubakov V., 2014, *J. Cosmol. Astropart. Phys.*, 1402, 019

- Klypin A., Kravtsov A. V., Valenzuela O., Prada F., 1999, *ApJ*, 522, 82
- Komatsu E. et al., 2011, *ApJS*, 192, 18
- Kravtsov A. V., Berlind A. A., Wechsler R. H., Klypin A. A., Gottlöber S., Allgood B., Primack J. R., 2004, *ApJ*, 609, 35
- Kuhlen M., Faucher-Giguère C.-A., 2012, *MNRAS*, 423, 862
- Laureijs R., et al, 2011, preprint (arXiv:1110.3193)
- Lewis A., Challinor A., 2000, *ApJ*, 538, 473
- Lorenzoni S., Bunker A. J., Wilkins S. M., Caruana J., Stanway E. R., Jarvis M. J., 2013, *MNRAS*, 429, 150
- Ma C.-P., Bertschinger E., 1995, *ApJ*, 455, 7
- Macciò A. V., Ruchayskiy O., Boyarsky A., Muñoz-Cuartas J. C., 2013, *MNRAS*, 428, 882
- McGreer I. D., Mesinger A., Fan X., 2011, *MNRAS*, 415, 3237
- McLure R. J. et al., 2013, *MNRAS*, 432, 2696
- Madau P., Haardt F., Rees M. J., 1999, *ApJ*, 514, 648
- Marsh D. J. E., Ferreira P. G., 2010, *Phys. Rev. D*, 82, 103528
- Marsh D. J. E., Silk J., 2013, *MNRAS*, 437, 2652
- Marsh D. J. E., Macaulay E., Trebitsch M., Ferreira P. G., 2012, *Phys. Rev. D*, 85, 103514
- Marsh D. J. E., Grin D., Hlozek R., Ferreira P. G., 2014b, *Phys. Rev. Lett.*, 113, 011801
- Marsh D. J. E., Pop, A., 2015, preprint (arXiv:1502.03456)
- Mesinger A., 2010, *MNRAS*, 407, 1328
- Moore B., Ghigna S., Governato F., Lake G., Quinn T., Stadel J., Tozzi P., 1999, *ApJ*, 524, L19
- Noh H., Park C.-G., Hwang J.-C., 2013, *Phys. Lett. B*, 726, 559
- Oesch P. A. et al., 2012, *ApJ*, 759, 135
- Oesch P. A. et al., 2009, *ApJ*, 690, 1350
- Pani P., Cardoso V., Gualtieri L., Berti E., Ishibashi A., 2012, *Phys. Rev. Lett.*, 109, 131102
- Park C.-G., Hwang J.-c., Noh H., 2012, *Phys. Rev. D*, 86, 083535
- Peccei R. D., Quinn H. R., 1977, *Phys. Rev. Lett.*, 38, 1440
- Peebles P. J. E., 1971, *Physical Cosmology*. Princeton Univ. Press, Princeton, NJ
- Planck Collaboration I, 2014a, *A&A*, 571, A1
- Planck Collaboration XVI, 2014b, *A&A*, 571, A16
- Planck Collaboration XIII, 2015, preprint (arXiv:1502.01589)
- Pospelov M., Ritz A., Skordis C., Ritz A., Skordis C., 2009, *Phys. Rev. Lett.*, 103, 051302
- Raffelt G., 2002, *Space Sci. Rev.*, 100, 153
- Reid B. A. et al., 2010, *MNRAS*, 404, 60
- Robertson B. E. et al., 2013, *ApJ*, 768, 71
- Schechter P., 1976, *ApJ*, 203, 297
- Schive H.-Y., Chiueh T., Broadhurst T., 2014, *Nat. Phys.*, 10, 496
- Schive H.-Y., Liao M-H, Woo T.-P., Wong S.-K., Chiueh T., Broadhurst T., Hwang W.-Y. P., 2014, *Phys. Rev. Lett.*, 113, 261302
- Schneider A., Anderhalden D., Maccio A., Diemand J., 2014, *MNRAS*, 441, L6
- Schultz C., Oñorbe J., Abazajian K. N., Bullock J. S., 2014, *MNRAS*, 442, 1597
- Sheth R. K., Tormen G., 1999, *MNRAS*, 308, 119
- Sikivie P., 2011, *Proc. Sci.*, POS(IDM2010)068
- Smith R. E., Markovic K., 2011, *Phys. Rev. D*, 84, 063507
- Spergel D., Flauger R., Hlozek R., 2013, preprint (arXiv:1312.3313)
- Stadnik, Y., Flambaum, V. V., 2014, *Mod. Phys. Lett. A*, 29, 1440007
- Steigman G., 2007, *Annu. Rev. Nucl. Part. Syst.*, 57, 463
- Sunyaev, R. A., Zel'dovich, I. B., 1980, *MNRAS*, 190, 413
- Svrcek P., Witten E., 2006, *J. High Energy Phys.*, 0606, 051
- Tremaine S., Gunn J. E., 1979, *Phys. Rev. Lett.*, 42, 407
- Turner M. S., 1983, *Phys. Rev. D*, 28, 1243
- Vale A., Ostriker J. P., 2004, *MNRAS*, 353, 189
- Viel M., Becker G. D., Bolton J. S., Haehnelt M. G., 2013, *Phys. Rev. D*, 88, 043502
- Wantz O., Shellard E. P. S., 2010, *Phys. Rev. D*, 82, 123508
- Weinberg S., 1978, *Phys. Rev. Lett.*, 40, 223
- White S. D., Frenk C., Davis M., 1983, *ApJ*, 274, L1
- Wilczek F., 1978, *Phys. Rev. Lett.*, 40, 279
- Willott C. J. et al., 2010, *AJ*, 139, 906
- Windhorst R. A., Cohen S. H., Jansen R. A., Conselice C., Yan H., 2006, *New Astron. Rev.*, 50, 113
- Witten E., 1984, *Phys. Lett. B*, 149, 351
- Wyse R. F. G., 2001, in Funes J. G., Corsini E. M., eds, *ASP Conf. Ser. Vol. 230, Galaxy Disks and Disk Galaxies*. Astron. Soc. Pac., San Francisco, p. 71
- Wyse R. F. G., Gilmore G., 2008, in Davies J. L., Disney M. J., eds, *Proc. IAU Symp. Vol. 244, Dark Galaxies and Lost Baryons*. Cambridge Univ. Press, Cambridge, p. 44
- Yan H., Windhorst R. A., 2004, *ApJ*, 612, L93